The contribution of host cell-directed vs. parasite-directed immunity to the disease and dynamics of malaria infections

Nina Wale[a,1], Matthew J. Jones[b], Derek G. Sim[b], Andrew F. Read[b,c,d], and Aaron A. King[a,e,f]

[a]Department of Ecology and Evolutionary Biology, University of Michigan, Ann Arbor, MI 48109; [b]Center for Infectious Disease Dynamics, Huck Institutes for the Life Sciences, Pennsylvania State University, University Park, PA 16802; [c]Department of Biology, Pennsylvania State University, University Park, PA 16802; [d]Department of Entomology, Pennsylvania State University, University Park, PA 16802; [e]Center for the Study of Complex Systems, University of Michigan, Ann Arbor, MI 48109; and [f]Department of Mathematics, University of Michigan, Ann Arbor, MI 48109

Edited by Ruslan Medzhitov, Yale University School of Medicine, New Haven, CT, and approved September 19, 2019 (received for review May 12, 2019)

Hosts defend themselves against pathogens by mounting an immune response. Fully understanding the immune response as a driver of host disease and pathogen evolution requires a quantitative account of its impact on parasite population dynamics. Here, we use a data-driven modeling approach to quantify the birth and death processes underlying the dynamics of infections of the rodent malaria parasite, *Plasmodium chabaudi*, and the red blood cells (RBCs) it targets. We decompose the immune response into 3 components, each with a distinct effect on parasite and RBC vital rates, and quantify the relative contribution of each component to host disease and parasite density. Our analysis suggests that these components are deployed in a coordinated fashion to realize distinct resource-directed defense strategies that complement the killing of parasitized cells. Early in the infection, the host deploys a strategy reminiscent of siege and scorched-earth tactics, in which it both destroys RBCs and restricts their supply. Late in the infection, a "juvenilization" strategy, in which turnover of RBCs is accelerated, allows the host to recover from anemia while holding parasite proliferation at bay. By quantifying the impact of immunity on both parasite fitness and host disease, we reveal that phenomena often interpreted as immunopathology may in fact be beneficial to the host. Finally, we show that, across mice, the components of the host response are consistently related to each other, even when infections take qualitatively different trajectories. This suggests the existence of simple rules that govern the immune system's deployment.

immune response | *Plasmodium chabaudi* | immunopathology | red blood cells | top-down vs. bottom-up control

When a pathogen infects a host, the host mounts a response to contain the pathogen and protect itself from harm. This response shapes the within-host ecological milieu in which pathogens proliferate and evolve and, in some cases, can directly contribute to host disease, a phenomenon known as immunopathology (1, 2). To fully understand host–parasite interactions, infection pathology, and host–parasite coevolution, we must therefore quantify the nature and dynamics of the host response to infection (3).

Yet, quantifying the impact of immunity on host and parasite fitness remains a challenge. Mechanistic approaches to the study of immunity, that characterize the host-cell populations involved and quantify the mechanisms responsible for changes in their abundance, distribution, and activity, have had many successes, including some that have informed vaccines and immunotherapeutic treatments. However, even equipped with an understanding of a cell type's function, it can be difficult to quantify that cell type's impact on parasite abundance or host symptoms as a function of its density (1, 4).

Here, we take a complementary approach that explicitly focuses on the net effects of the host response on births and deaths of host and parasite cells, which, in turn, directly affect host health and parasite fitness. Specifically, we decompose the host response to the mouse malaria parasite, *Plasmodium chabaudi*, into qualitatively distinct components that variously kill parasites or control their access to resources. We use a data-driven approach to extract the time course of each component from experimental data and then compute the impacts of each on both host symptoms (i.e., anemia) and parasite proliferation. In so doing, we paint a quantitative picture of the host response as both a driver of disease and a selective pressure on parasites. We examine how the trajectories of the distinct components relate to parasite burden and to each other and formulate hypotheses as to how and to what end they are deployed. By thus focusing on the effects of the host response as distinct from effectors that mediate it, we elucidate the strategies a host employs to control an infection as distinct from the weaponry it uses to achieve them.

Results

Decomposition of the Host Response. We developed a simple, semimechanistic approach to infer the nature and shape of the host response to malaria infections from experimental data (*Materials and Methods*). We take advantage of *P. chabaudi*'s synchronous, daily life cycle: Every 24 h, these parasites invade,

Significance

What makes an infected host sick—the pathogen or the host response to it? How should pathogens defend themselves? Answering these questions requires an understanding of how, and how much, the immune response changes populations of host and pathogen cells. We break down the immune response into components with distinct effects on cell birth and death, and quantify the impact of each on disease and pathogens. We find that hosts control infections not only by killing pathogens, but by starving parasites and shortening the lifespans of cells on which they depend. This work reveals that some immune responses—often seen as harmful to the host—may in fact be helpful and suggests simple rules that govern the immune response's deployment.

Author contributions: N.W. and A.A.K. designed research; N.W., M.J.J., D.G.S., and A.A.K. performed research; N.W. and A.A.K. analyzed data; N.W. and A.A.K. wrote the paper; A.F.R. provided laboratory resources, personnel, and protocols; and M.J.J., D.G.S., and A.F.R. provided comments on the manuscript.

The authors declare no competing interest.

This article is a PNAS Direct Submission.

Data deposition: Data and code related to this paper have been deposited in Dryad (DOI: 10.5061/dryad.nk98sf7pk).

[1]To whom correspondence may be addressed. Email: nwale@umich.edu.

This article contains supporting information online at www.pnas.org/lookup/suppl/doi:10.1073/pnas.1908147116/-/DCSupplemental.

First published October 15, 2019.

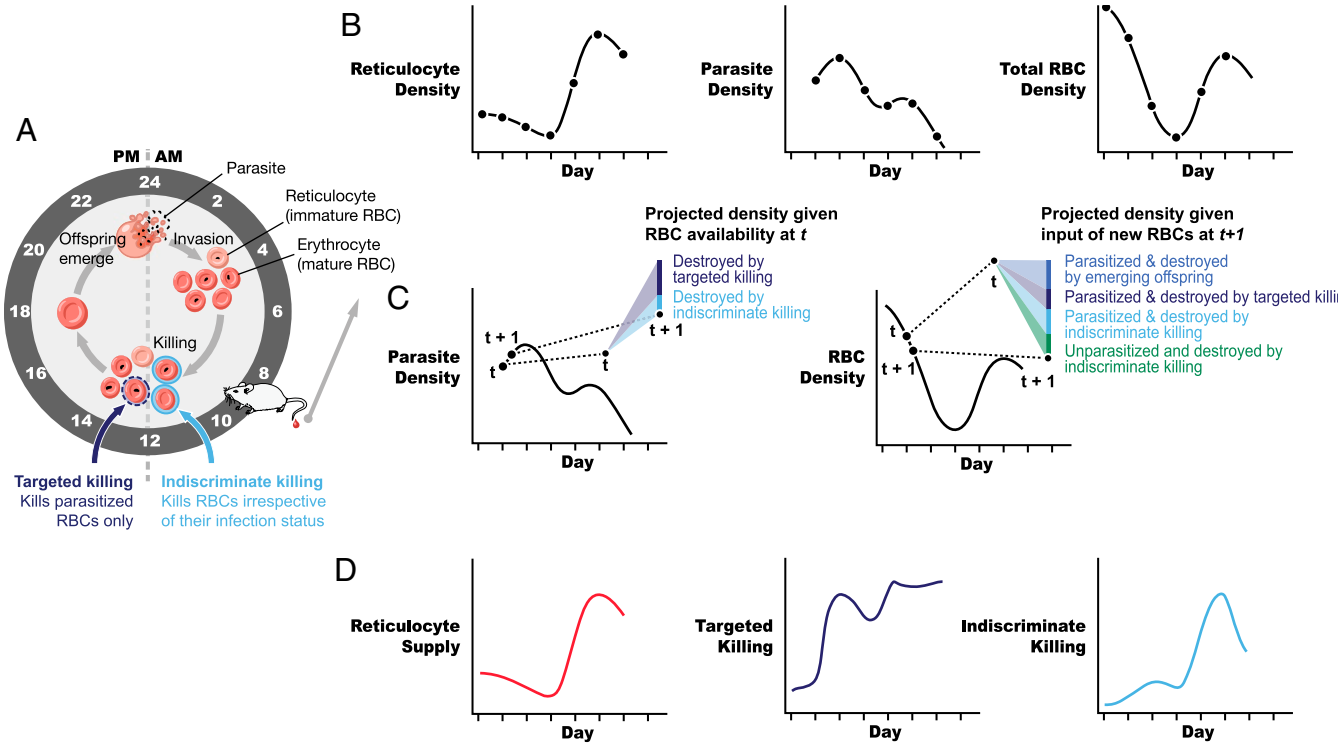

Fig. 1. Decomposing the host immune response. (*A*) The daily cycle of malaria parasites in the blood stage of infection. Each day, parasite offspring (merozoites) burst from RBCs and then attempt to invade new RBCs, wherein they mature and reproduce. In our model, the host immune response modulates infection by killing RBCs and adjusting their supply. Samples were taken from experimentally infected mice each morning, before parasites had reproduced, and were processed to produce time-series data on infection dynamics (see *B*). (*B*) Time series of reticulocyte (i.e., immature RBC), parasite, and total (mature + immature) RBC densities. (*C*) Eq. **1** shows how these 3 data streams can be transformed into 3 synthetic variables (components of the immune response), which describe the impacts of the immune response on parasite proliferation and host health (anemia). In particular, RBCs can be killed by a response targeted at parasitized cells or by a response that kills RBCs irrespective of their infection status. Moreover, the host can modulate the supply of reticulocytes. The model works by projecting the density of RBCs and parasites at the next time step ($t + 1$) in the absence of any killing, given the abundance of RBCs and parasites at time t and the supply of RBCs at time $t + 1$. The deficit between these projections and the data is then partitioned among the indiscriminate and targeted killing components. (*D*) This procedure yields, for each infected mouse, time series of the 3 immune-response components. By comparing these trajectories across mice, we identify robust patterns which can be interpreted in terms of host defense strategy.

reproduce, and burst out of red blood cells (RBCs), which are destroyed in the process (Fig. 1*A*). With measures of the densities of parasites and RBCs, together with the rate at which immature RBCs (reticulocytes) are supplied to the bloodstream (Fig. 1*B*), and supposing that parasite reproduction is limited by RBC availability alone, one can forecast how many parasitized and unparasitized RBCs should be present a day later. Observed deviations from this forecast can thence be attributed either to a host response targeted at parasitized cells ("targeted killing") or to one that removes RBCs irrespective of their infection status ("indiscriminate killing"; Fig. 1*C* and *Materials and Methods*). Repeatedly applying this process to time-series data collected from experimental infections, we deduced the trajectories of each of 3 functionally distinct, time-varying components (Fig. 1*D*): targeted killing, indiscriminate killing, and (restriction of) RBC supply.

We applied this approach to data (densities of reticulocytes, total RBCs, and parasites) collected daily from 12 experimentally infected and 3 uninfected mice of the same genetic background (*SI Appendix*, Fig. S1). To generate variability in the infection dynamics among the mice, they were split into 4 groups, each of which was supplied with a different concentration of a nutrient (*para*-aminobenzoic acid [pABA]) that alters the growth rate and dynamics of parasite populations but is not needed by the host (5, 6). For brevity, in the main text, we show and analyze data from the same 3 mice, each of which was given a different concentration of the nutrient; the complete data and analysis of all mice can be found in *SI Appendix*.

Mice exhibited markedly different infection dynamics. As expected, the initial growth rate of infections increased with the concentration of pABA that they were administered ($F_{3,29} = 5.4$; $P < 0.01$). Furthermore, while some mice experienced severe anemia—i.e., pathologically low numbers of RBCs (e.g., Fig. 2*A*, mouse 1)—or displayed a "shoulder" in the postpeak phase of the infection (e.g., Fig. 2*A*, mice 1 and 2), others did not (e.g., Fig. 2*A*, mouse 3).

The model was sufficiently flexible that the dynamics of infection of all mice were well captured (Fig. 2 *A*–*C*). Despite the variation in infection dynamics, the trajectories of the 3 response components were qualitatively similar across mice (Fig. 2*D*). These functions were scaled to be commensurate with RBC densities, so that their magnitudes relative to RBC density determined the fate of RBCs and parasites (cf. Eq. **1**). In the prepeak phase (~0 to 7 d), the targeted response increased rapidly and peaked in concert with parasite density, while the indiscriminate response showed no discernible trend. Meanwhile, the supply of reticulocytes went unchanged or even, in some cases, fell. Following the peak in parasite density, the targeted response fell as the indiscriminate response and reticulocyte supply increased. Strikingly, the trajectories of the latter 2 components moved in tandem during this period (Fig. 2*D*). Once RBC numbers recovered (approximately day 15), the indiscriminate and

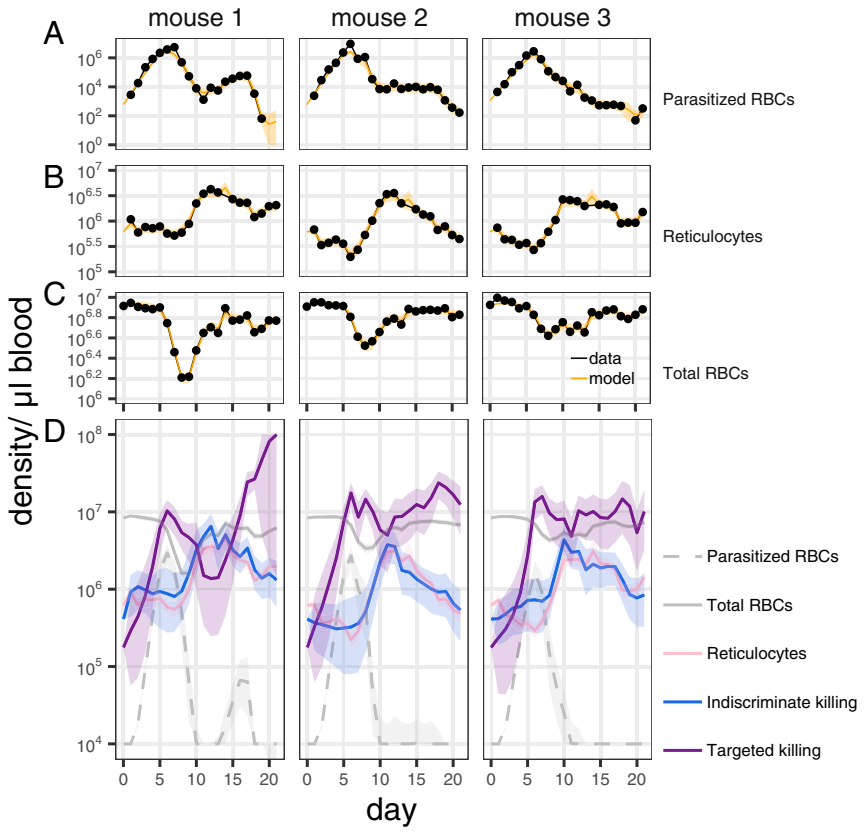

Fig. 2. The model accurately captures the data and yields the dynamics of 3 qualitatively distinct host responses. (*A*–*C*) Measured (black) and fitted (orange) densities of parasitized RBCs (*A*), reticulocytes (*B*), and total RBCs (*C*) in 3 mice which were (left to right) fed a 0.005% concentration, 0.0005% concentration, and a 0% solution of pABA, a nutrient that stimulates parasite growth rate. Data and fitted model trajectories for all mice are shown in *SI Appendix*, Figs. S1 and S2. (*D*) Estimated trajectories of 3 distinct host responses that target parasitized cells only ("targeted killing"; purple) and RBCs irrespective of their infection status (indiscriminate killing; blue) and that resupply reticulocytes (pink). Note that these responses are of the same order of magnitude as the RBCs. Plotted are the mean (solid line) and 90% confidence interval (ribbon) on the smoothed estimate of the model trajectories.

supply responses decreased in magnitude, and the targeted response increased once again.

Parsing the Effect of the Host Response on Pathology and Parasite Fitness. To better understand the impact of each of the response components on parasite fitness and host disease, and hence to identify putative host defense strategies, we quantified the effect of each response component on parasite destruction and on anemia (Fig. 3).

At the infection's outset, parasite populations grew at near their maximum rate, and the majority of parasite offspring emerged from mature RBCs (erythrocytes). Very rapidly, however, parasites were unable to realize their reproductive potential due to the combined impacts of the targeted response and RBC limitation. At its maximum, RBC limitation accounted for, on average, a 22% (interdecile range, 12 to 33%) reduction in parasite reproductive potential (Fig. 3*A*).

RBC limitation resulted from RBC destruction by the parasite and the host, as well as the restriction of RBC supply. Together, these 3 forces induced anemia. Notably, only a small fraction of RBC losses were attributable to parasites bursting from RBCs (Fig. 3*C*). Even when the contribution of parasite emergence to RBC destruction was at its height, it was never responsible for more than half of the RBC destruction (maximum [across time] proportion of losses attributable to parasite emergence, mean [among mice] 33% interdecile range 18 to 43%). Rather, most RBC losses were due to the indiscriminate response, which removed both parasitized and unparasitized cells. At the beginning of the infection, almost all of the losses of RBCs could be attributed to the removal of unparasitized cells by the indiscriminate response (mean, 99.5%; interdecile range, 99 to 100%), and, indeed, there were only a few days, around the time of peak parasite density, when the host killed more parasitized than unparasitized cells. On these days, 4 parasitized cells were removed on average for every 1 unparasitized cell (interdecile range 1.3 to 9). In addition, the restriction of reticulocyte supply exacerbated anemia, as each day's supply of new RBCs failed to compensate for the previous day's losses (Fig. 3*B*). Strikingly, despite incurring huge losses in RBCs, infected mice did not increase the supply of reticulocytes any more than did uninfected mice in the first 8 d of infection (Fig. 2; total reticulocyte count, days 0 to 8, $F_{1,13} = 3.2$, $P = 0.1$). Metaphorically speaking, the restriction of RBC supply and the killing of uninfected RBCs represent "siege" and "scorched earth" strategies, respectively, which combined to limit the resources available to the parasite and make the host sick. These strategies supplemented the "slaughter" of infected cells by the targeted response to bring the parasite population under control.

The postpeak phase of infection, in which parasite numbers declined and mice recovered from anemia, was characterized by an increase in the magnitude of the indiscriminate response. At its peak, this response component was responsible for 53% (interdecile range 38 to 70%) of parasite destruction on average (Fig. 3*A*), as well as the destruction of many unparasitized RBCs.

Despite this postpeak increase in indiscriminate killing, the mouse recovered from anemia. This was due to the concomitant

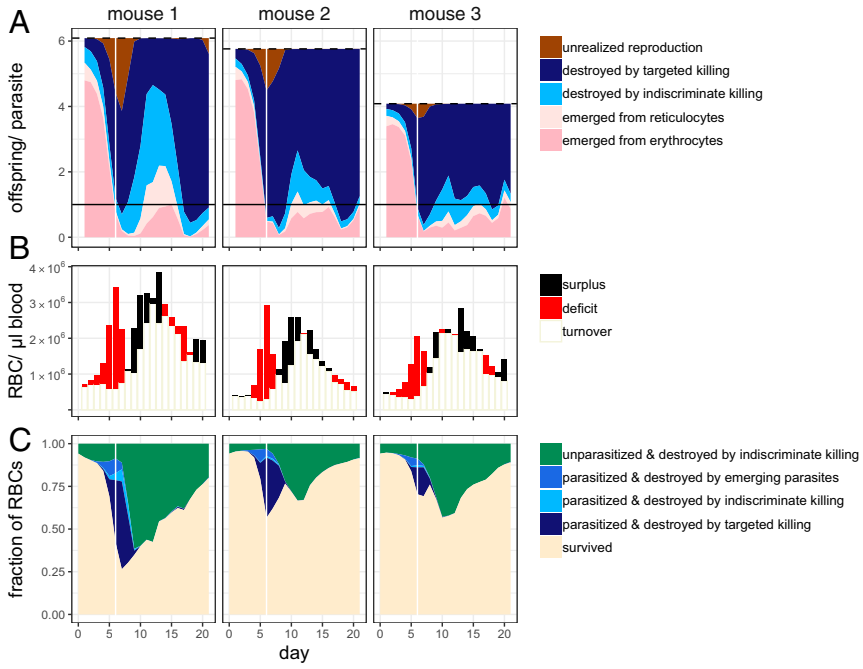

Fig. 3. Contribution of the different components of the host response to parasite fitness and host disease. (*A*) Contribution of the host to the (suppression of) parasite reproduction in 3 different mice (left to right), each of which was fed a different concentration of a nutrient that stimulates parasite growth. The dashed line indicates the maximum number of offspring that could be produced per parasitized cell in conditions of unlimited RBC availability; the fill area indicates the estimated number of offspring that successfully emerged (pinks), were destroyed by each of the killing responses (blues), or were not produced due to the limited availability of RBCs (brown). The black horizontal line indicates 1 offspring/parasite: When the blue area descends below this line, the parasite population is decreasing in size. (*B*) The uncolored part of the bar indicates the number of the previous day's losses that were compensated for by the present day's supply of reticulocytes (turnover); the colored section indicates the extent to which the present day's supply of reticulocytes exceeded yesterday's losses ("surplus"; black) or failed to compensate for them ("deficit"; red). (*C*) The relative contribution of parasites and each of the host responses to the fate of RBCs through time. Note that parasites can contribute to RBC destruction directly, by emergence, or indirectly via the targeted killing response. The white vertical line in *A* and *C* indicates the time of peak parasite density. Shown are the decompositions for the same 3 mice used in all other figures. Equivalent plots for the 9 other mice analyzed can be found in *SI Appendix*, Fig. S3.

increase in the supply of reticulocytes, which more than compensated for the destruction of RBCs (Fig. 3*B*). In contrast to the prepeak phase, here, the host controlled parasite population growth not by making RBCs scarce, but by altering their demographic profile. Specifically, because the indiscriminate response increased in tandem with reticulocyte supply, the combined effect was to increase the turnover rate of RBCs, markedly reducing their average age. Thus, although RBCs became more abundant, parasites that successfully invaded an RBC still had a low probability of reproducing, since the RBC that they had invaded was likely to be cleared before they did so. Strategically speaking, this "juvenilization" strategy allows the host to recover from anemia while restraining parasite growth.

In the final phase (days 15 to 21), both the indiscriminate killing and supply responses returned to roughly their initial levels. The targeted response, by contrast, remained at heightened levels and, in some cases, increased.

Coordination of the Host Response. Though infection dynamics vary among mice, the components of the host response followed stereotypical trajectories (Fig. 2*D*). This suggests that the components may be deployed in a coordinated manner. To investigate this possibility, we plotted the trajectories of each response against one another and against parasite density. This analysis revealed that the infection rolled out in 3 phases, separated by 2 landmarks (denoted **a** and **b** in Fig. 4).

In the first phase, the targeted response grew with the parasite population, as the reticulocyte supply fell and the indiscriminate response slowly grew. At landmark **a**, the parasite population and targeted killing response stopped growing and began to decrease. Notably, there was no time lag between the fall in parasite density and the fall in the targeted killing response (Fig. 4*A*). Landmark **a** also marks the point where the magnitude of the reticulocyte supply and indiscriminate killing responses became tightly correlated, growing and waning with each other for the duration of the infection (Fig. 4*C*). Landmark **b** marks the beginning of a third phase, where the indiscriminate response reached its peak and began to fall, along with the supply of reticulocytes. The growth rate of the parasite population and targeted killing response became decoupled and their trajectories more idiosyncratic in this phase. While the targeted response tended to grow during this latter phase, only in some mice did parasite density stop falling or grow again, so as to form a "shoulder" in the parasite density curve, before finally falling to undetectable levels.

Discussion

Understanding the character and dynamics of the host response to infection is essential if we are to apportion responsibility for pathology between parasite and host, elucidate the role of the immune response in shaping parasite traits, and, ultimately, predict the dynamics of infections. Here, we used a simple accounting scheme to decompose the host response into 3 functionally distinct components and to infer their respective dynamics. This decomposition allows us to formulate hypotheses regarding the strategic significance of aspects of the immune response.

Our analysis suggests that host responses to infection that have been interpreted as immunopathology may in fact serve as effective defense strategies. The restriction of the supply of reticulocytes to the bloodstream at the outset of malaria infections, the accelerated clearance of erythrocytes toward the end of infections, and the destruction of uninfected erythrocytes

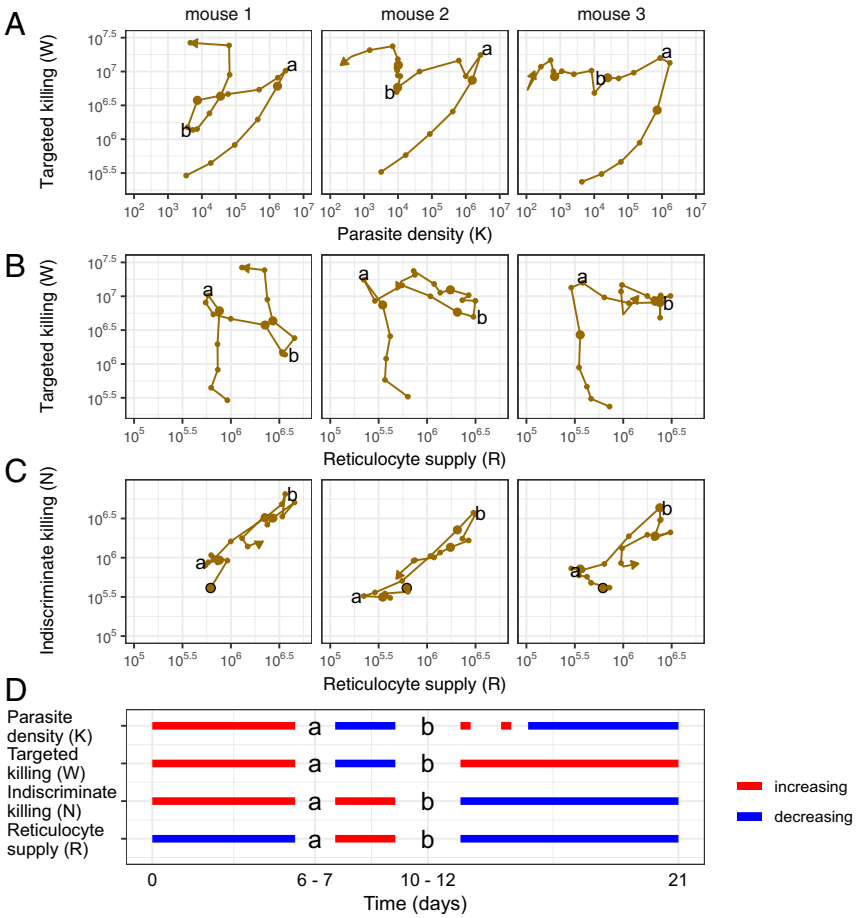

Fig. 4. The components of the immune response are similarly deployed, even among mice displaying different infection dynamics. (*A*–*C*) The relationships between the 3 components of the host response. The large, black-outlined dot indicates the starting point of the infection. Each subsequent day is marked with a dot, with large dots indicating days 5, 10, 15, and 20. Landmarks **a** and **b** identify transitions between regimens of deployment of the components that occur, as summarized in *D*. (NB: The timing of these landmarks is consistent across all mice in the analysis, with the exception of 2 mice that received fewer parasites than intended; *SI Appendix*, Figs. S1 and S4.) (*D*) The dashed red line indicates that parasite density increases in some, but not all, mice during the period indicated. Densities of parasites and RBCs are in units per microliter of blood. These trajectories are from the same 3 mice whose infections are displayed in Figs. 2 and 3, each of which received a different concentration of pABA, a nutrient that alters parasite growth rate.

are well-known features of malaria infections in primates and rodents (e.g., refs. 7–11). Each have, at times, been interpreted as pathological. For example, restricted erythropoiesis has been dubbed "inappropriate" or "ineffective" erythropoiesis in the literature (7, 12). Our analysis provides evidence that, while these phenomena do contribute to the anemia of malaria infections (Fig. 3 *B* and *C*), they also contribute importantly to the control of parasite populations. In particular, early in an infection, the restriction of reticulocyte supply and the destruction of uninfected cells shrink the reproductive potential of parasites; in the later phase, increased RBC clearance, in conjunction with augmented erythropoiesis, accelerates blood compartment turnover, thereby reducing parasite survival while allowing the host to recover. Our analysis thus illustrates the general principle that, in evaluating whether a given component of the host response is pathological or not, one must consider it in the context of other, simultaneously mounted, responses and its effects on parasite fitness as well as host disease. Indeed, some aspects of illness may, when considered in this way, prove to be adaptive (13).

The relative contributions of resource limitation ("bottom-up control") and direct killing ("top-down control") to the dynamics of malaria infections have been hotly debated, with several authors suggesting that RBC limitation alone is sufficient to explain infection dynamics in the acute phase (14–16). While our model is flexible enough to encompass such an explanation, we find that the model most consistent with the data is one in which the host slows parasite population growth in the acute phase by a combination of resource limitation and direct removal of parasitized cells. We suspect that this discrepancy with previous findings arises from our use of explicit measurements of reticulocyte supply, where previous efforts relied on model assumptions. Similarly, the absence of data on reticulocyte abundance in previous studies likely explains why resource turnover has not been previously highlighted as an important mechanism of regulating malaria infections. To further examine the role of resource limitation in limiting parasite growth, we suggest that experimental manipulation of RBC densities be performed. For example, our work predicts that the transfusion of RBCs would not significantly boost parasite densities, except during the short period where resource limitation significantly impacts parasite fitness (i.e., within the 4- to 5-d window surrounding the peak in parasite density; Fig. 3*A*).

Though there was variation in the relative contribution of the different components of the host response to infection dynamics, the relationships between these components were consistent across mice, suggesting that simple, predictive models of infection dynamics might be built based on this work. Interestingly,

we uncovered patterns of coregulation that contravened the standard assumptions of many models of within-host infection dynamics. Specifically, mechanistic models of immunity have commonly described the immune response as a predator–prey interaction, whereby the immune response (the "predator") grows as a function of the density of the infected cells (the "prey") (17–19). Our analysis (Fig. 4) shows that the waxing and waning of the targeted killing response is not a function of parasite abundance alone. A broader class of models may thus be required to accurately capture the within-host dynamics of infections.

A complete understanding of the immune response requires that we not only map its effects on parasite and host cells, as we do here, but also understand the mechanisms that mediate those effects. Intriguingly, not only does our model describe phenomena common in the malaria literature (see above), but the patterns of coregulation echo findings in the wider immunological literature. For example, the antagonism between the parasite-killing response/parasite density and the supply response (Fig. 4*D*) is reminiscent of the antagonism of erythropoiesis by TNFα and hemozoin, which halt the production of reticulocytes (20, 21).

The identification of the mechanisms underlying observed patterns is unlikely to be routinely straightforward, however. We expect that, in general, multiple cell types and signaling molecules will mediate the responses we describe. For example, there are several mechanisms that might be responsible for the increased removal of uninfected cells during malaria infections (8, 22, 23). Experimental manipulation of infection dynamics, in combination with measurements of a panel of putative mediators [as per the procedures used in systems immunology (24)], has the potential to tease apart which of the array of cell types are the most sensitive predictors of each of the different components of the host response that we describe. Population-level approaches, such as ours, that focus on the quantitative effects of the immune response are an invaluable complement to cellular-level approaches focused on immune mechanisms. By combining these approaches, we stand to gain a holistic understanding of infection and immunity.

Materials and Methods

Hosts and Parasites. Hosts were 15 6- to 8-wk-old C57BL/6J female mice. Twelve mice were infected intraperitoneally with 10^6 *P. chabaudi* parasites of the pyrimethamine-resistant AS_{124} strain; 3 were left uninfected but received a sham injection of dimethyl sulfoxide to control for effects of receiving an injection. To create variation in infection dynamics, 3 mice were assigned to each of 4 treatments that received a 0.05%, 0.005%, 0.0005%, or 0% solution of pABA as drinking water, from a week before parasites were inoculated. Uninfected mice received a 0% pABA solution as drinking water.

Infection Monitoring. Infections were monitored daily from the day of inoculation (day 0) to day 21 postinoculation. A total of 14 μL of blood was taken from the tail: 5 μL for the assessment of parasite density via qPCR and 2 μL for the quantitation of total RBC density via a Coulter Counter (Beckman Coulter), as described (5). A further 2 μL was used for the quantitation of the relative abundance of reticulocytes (young RBCs) and erythrocytes (mature RBCs) via flow cytometry (*SI Appendix*), and the remainder of blood for other assays not described herein. The density of reticulocytes and erythrocytes was calculated by multiplying their respective proportions in the blood by the total RBC density.

Model Structure. To decompose the host response to infection, we formulated a model of the interaction among RBCs, parasites, and 3 host-response components. The model tracked the concentrations of erythrocytes, E_t; reticulocytes, R_t; and merozoites (parasite offspring), M_t, as functions of time t. Given these quantities, together with the values on day t of the targeted and indiscriminate killing responses (W_t and N_t, respectively), the model postulates that

$$\begin{aligned} K_t &= (R_t + E_t)\left(1 - \exp\left(-\frac{M_t}{R_t + E_t}\right)\right) \\ M_{t+1} &= \beta K_t \exp\left(-\frac{W_t + N_t}{R_t + E_t}\right) \\ E_{t+1} &= (R_t + E_t)\exp\left(-\frac{M_t + N_t}{R_t + E_t}\right), \end{aligned} \quad [1]$$

where K_t is the concentration of parasitized RBCs. Following empirical work (25, 26), we assumed that all RBCs were equally susceptible to the parasite. According to Eq. **1**, each of the K_t parasitized cells contributes β merozoites to the population of day $t+1$, if it is not first removed by 1 of the 2 killing responses (N_t and W_t). Note that the magnitudes of the killing responses are expressed in units of RBC density. The third host-response component is the supply of new reticulocytes into the bloodstream, R. We assume that reticulocytes mature into erythrocytes in precisely 1 d (27). The form of Eq. **1** arises as the expectation of a stochastic urn process whereby each RBC faces a chance of becoming parasitized or destroyed by the host response in proportion to the relative abundances of W_t, N_t, and M_t. As such, Eq. **1** is deterministic, conditional on N_t, W_t, and R_t. Stochasticity enters the model via the assumption that these variables are Gaussian Markov random fields (GMRFs), with respective standard deviations σ_N, σ_W, and σ_R. Finally, the variables R, E, and K are related to the data via an explicit model of measurement errors. Specifically, measurements of parasite, reticulocyte, and total RBC densities on day t are assumed to be log-normally distributed around their true values (K_t, R_t, and $E_t + R_t$, respectively).

Model Fitting and Smoothing. The model has the form of a partially observed Markov process (28), for which efficient inference algorithms have been implemented. Since our mice were inbred and of the same age, we assumed that they shared values of the GMRF parameters σ_N, σ_W, and σ_R as well as the initial conditions E_0, R_0, W_0, and N_0 and measurement errors σ_{Pd}, σ_{Retic}, and σ_{RBC}. Since pABA concentration affects parasite reproduction rate, we estimated a common value of β for each pABA treatment, but allowed each mouse its own inoculum size, to account for experimental variation in parasite injection volume and to allow the inclusion of data from 2 mice that received fewer parasites than was intended. We estimated inoculum size and β via multiple linear regression applied to the first 4 d of data. We estimated the remaining 10 parameters (σ_N, σ_W, σ_R, σ_{Pd}, σ_{Retic}, and σ_{RBC}, plus the initial conditions E_0, R_0, W_0, and N_0) using the IF2 algorithm (29) as implemented in the R packages pomp (28, 30) and panelPomp (31). Further details about model fitting can be found in *SI Appendix*.

ACKNOWLEDGMENTS. We thank James Fraser, the Huck Institutes Flow Cytometry Facility (both at Pennsylvania State University), and David Adams (University of Michigan) for assistance with the design and implementation of the flow cytometry protocol; and the members of the A.A.K., Woods, and Zaman groups (University of Michigan) for comments on the manuscript. This work was supported by NIH Grants R01AI101155 and U54GM111274 (to A.A.K.) and by an NSF-supported Infectious Disease Evolution Across Scales Research Coordination Network research exchange grant (to N.W.).

1. M. E. Hochberg, An ecosystem framework for understanding and treating disease. *Evol. Med. Public Health* **2018**, 270–286 (2018).
2. A. L. Graham, J. E. Allen, A. F. Read, Evolutionary causes and consequences of immunopathology. *Annu. Rev. Ecol. Evol. Syst.* **36**, 373–397 (2005).
3. S. M. Hedrick, Understanding immunity through the lens of disease ecology. *Trends Immunol.* **38**, 888–903 (2017).
4. R. Zinkernagel, On observing and analyzing disease versus signals. *Nat. Immunol.* **8**, 8–10 (2007).
5. N. Wale, D. G. Sim, A. F. Read, A nutrient mediates intraspecific competition between rodent malaria parasites in vivo. *Proc. R. Soc. Biol. Sci.* **284**, 20171067 (2017).
6. P. F. Fenton, G. R. Cowgill, M. A. Stone, D. H. Justice, The nutrition of the mouse. 8. Studies on pantothenic acid, biotin, inositol and p-aminobenzoic acid. *J. Nutr.* **42**, 257–269 (1950).
7. K. H. Chang, M. M. Stevenson, Malarial anaemia: Mechanisms and implications of insufficient erythropoiesis during blood-stage malaria. *Int. J. Parasitol.* **34**, 1501–1516 (2004).
8. M. G. Salmon, J. B. De Souza, G. A. Butcher, J. H. L. Playfair, Premature removal of uninfected erythrocytes during malarial infection of normal and immunodeficient mice. *Clin. Exp. Immunol.* **108**, 471–476 (1997).
9. G. N. Jakeman, A. Saul, W. L. Hogarth, W. E. Collins, Anaemia of acute malaria infections in non-immune patients primarily results from destruction of uninfected erythrocytes. *Parasitology* **119**, 127–133 (1999).
10. S. Looareesuwan *et al.*, Reduced erythrocyte survival following clearance of malarial parasitaemia in Thai patients. *Br. J. Haematol.* **67**, 473–478 (1987).
11. S. Looareesuwan *et al.*, Erythrocyte survival in severe falciparum malaria. *Acta Trop.* **48**, 263–270 (1991).

12. K. Deroost, T.-T. Pham, G. Opdenakker, P. E. Van den Steen, The immunological balance between host and parasite in malaria. *FEMS Microbiol. Rev.* **40**, 208–257 (2016).
13. P. W. Ewald, *Evolution of Infectious Disease* (Oxford University Press, Oxford, U.K., 1994).
14. R. Antia, A. Yates, J. C. de Roode, The dynamics of acute malaria infections. I. Effect of the parasite's red blood cell preference. *Proc. R. Soc. Lond. Ser. B Biol. Sci.* **275**, 1449–1458 (2008).
15. N. Mideo *et al.*, Understanding and predicting strain-specific patterns of pathogenesis in the rodent malaria *Plasmodium chabaudi*. *Am. Nat.* **172**, 214–238 (2008).
16. C. J. E. Metcalf *et al.*, Partitioning regulatory mechanisms of within-host malaria dynamics using the effective propagation number. *Science* **333**, 984–988 (2011).
17. G. I. Bell, Predator-prey equations simulating an immune response. *Math. Biosci.* **16**, 291–314 (1973).
18. D. Wodarz, Ecological and evolutionary principles in immunology. *Ecol. Lett.* **9**, 694–705 (2006).
19. A. Fenton, S. E. Perkins, Applying predator-prey theory to modelling immune-mediated, within-host interspecific parasite interactions. *Parasitology* **137**, 1027–1038 (2010).
20. I. A. Clark, G. Chaudhri, Tumour necrosis factor may contribute to the anaemia of malaria by causing dyserythropoiesis and erythrophagocytosis. *Br. J. Haematol.* **70**, 99–103 (1988).
21. C. Casals-Pascual *et al.*, Suppression of erythropoiesis in malarial anemia is associated with hemozoin *in vitro* and *in vivo*. *Blood* **108**, 2569–2577 (2006).
22. I. Safeukui *et al.*, Malaria induces anemia through CD8+ T cell-dependent parasite clearance and erythrocyte removal in the spleen. *mBio* **6**, e02493-14 (2015).
23. C. Fernandez-Arias *et al.*, Anti-self phosphatidylserine antibodies recognize uninfected erythrocytes promoting malarial anemia. *Cell Host Microbe* **19**, 194–203 (2016).
24. M. M. Davis, C. M. Tato, D. Furman, Systems immunology: Just getting started. *Nat. Immunol.* **18**, 725–732 (2017).
25. W. Jarra, K. N. Brown, Invasion of mature and immature erythrocytes of CBA/Ca mice by a cloned line of *Plasmodium chabaudi chabaudi*. *Parasitology* **99**, 157–163 (1989).
26. G. S. Yap, M. M. Stevenson, Blood transfusion alters the course and outcome of *Plasmodium chabaudi* AS infection in mice. *Infect. Immun.* **62**, 3761–3765 (1994).
27. P. A. Ney, Normal and disordered reticulocyte maturation. *Curr. Opin. Hematol.* **18**, 152–157 (2011).
28. A. A. King, D. Nguyen, E. L. Ionides, Statistical inference for partially observed Markov processes via the R package pomp. *J. Stat. Softw.* **69**, 1–43 (2016).
29. E. L. Ionides, D. Nguyen, Y. Atchadé, S. Stoev, A. A. King, Inference for dynamic and latent variable models via iterated, perturbed Bayes maps. *Proc. Natl. Acad. Sci. U.S.A.* **112**, 719–724 (2015).
30. A. A. King *et al.*, pomp: Statistical inference for partially observed Markov processes, R package, Version 2.0.13.1. https://kingaa.github.io/pomp/. Accessed 19 August 2019.
31. C. Bretó, E. L. Ionides, A. A. King, Panel data analysis via mechanistic models. *J. Am. Stat. Assoc.*, 10.1080/01621459.2019.1604367 (2019).

PNAS
www.pnas.org

Supplementary Information for

The contribution of host cell-directed vs. parasite-directed immunity to the disease & dynamics of malaria infections.

Nina Wale, Matthew J. Jones, Derek G. Sim, Andrew F. Read, Aaron A. King

Corresponding Author Nina Wale.
E-mail: nwale@umich.edu

This PDF file includes:

www.pnas.org/cgi/doi/10.1073/pnas.1908147116

Supporting Information Text

Experimental methods: further details

Assaying RBC demography using flow cytometry. We used flow cytometry to measure the proportion of reticulocytes (young RBCs) and erythrocytes (mature RBCs) in the blood. Reticulocytes express the CD71 receptor, which is lost upon their maturation into erythrocytes (1, 2); all cells in the erythroid lineage express the TER119 antigen (3). Thus, staining with distinctly-tagged TER-119 and CD71 antibodies can be used to isolate the RBC portion of the blood and measure the relative abundance of reticulocytes and erythrocytes (4).

Blood was stained with TER-119 and CD71 antibodies labelled with distinct fluorophores. Briefly, 2 µl blood was collected in 48 µl running buffer (phosphate buffer saline with 2 mM Ethylenediaminetetraacetic acid and 2% fetal bovine serum). Cells were mixed with 50 µl of each of three different solutions: FITC anti-mouse CD71 (Biolegend 113805), PE anti-mouse TER-119 (Biolegend 116207), APC anti-mouse CD41 (Biolegend 133914), for final concentrations of 0.005, 0.0025, and 0.0025 µg/µl, respectively. Samples were vortexed and incubated for an hour at 4C in the dark, washed with 1 ml of running buffer and centrifuged at 2000 rpm for 5 min. The supernatant was then decanted and the pellet resuspended to a final concentration of 10^7 cells/µl.

Stained samples were analyzed using a FlowSight Imaging Flow Cytometer (Amnis) with specifications described in Table S-1. 300,000 events were counted per sample and analysis performed using IDEAS software (Amnis, version 6), as follows. RBCs were distinguished from platelets and cell debris by their size (area) and $CD41^-$ status. Single cells were then distinguished from doublets on the basis of their major axis (the longest dimension of the cell) and density (side-scatter). The population of single, $TER119^+$ cells was then plotted in TER119/CD71 space and reticulocytes ($CD71^+$) cells gated from erythrocytes ($CD71^-$) using a gate drawn using fluorescence minus one (FMO) controls (RBCs stained with the CD41 and TER119 antibodies but not CD71). Single color (1000 events), FMO and unstained (5000 events) controls were generated from the blood of uninfected mice and run prior to sample analysis, daily. On days 11–14 samples were not stained with the CD41 antibody, as this reagent was unavailable.

We multiplied daily measures of the proportion of reticulocytes and erythrocytes, as derived as above, by the total RBC density to obtain the density of reticulocytes and erythrocytes on each day (Fig. S-1).

Mathematical modeling: further details

Calculating the contribution of the different host response components to parasite fitness and host disease. We begin by making the definitions

$$S_t^M = \exp\left(-\frac{M_t}{R_t+E_t}\right), \qquad S_t^N = \exp\left(-\frac{N_t}{R_t+E_t}\right),$$
$$S_t^W = \exp\left(-\frac{W_t}{R_t+E_t}\right).$$

Now, to quantify the relative contribution of the indiscriminate killing response, targeted response, and parasites to RBC destruction (as shown in Figs. 3C & S-3), we calculate the following quantities that collectively sum to 1:

$$\begin{aligned}
Q_t^{ps} &= \left(1-S_t^M\right)\, S_t^W\, S_t^N,\\
Q_t^{pn} &= \frac{N_t}{N_t+W_t}\,\left(1-S_t^M\right)\,\left(1-S_t^W\, S_t^N\right),\\
Q_t^{pw} &= \frac{W_t}{N_t+W_t}\,\left(1-S_t^M\right)\,\left(1-S_t^W\, S_t^N\right),\\
Q_t^{un} &= S_t^M\,\left(1-S_t^N\right),\\
Q_t^{us} &= S_t^M\, S_t^N.
\end{aligned}$$

Here, Q_t^{ps} is the fraction of RBCs infected and destroyed by parasites emerging from them, Q_t^{pn} the fraction parasitized and destroyed by indiscriminate killing, Q_t^{pw} the fraction parasitized and destroyed by targeted killing, Q_t^{un} the fraction that go uninfected but are nevertheless destroyed by indiscriminate killing, and Q_t^{us} is the fraction of RBCs that survive in the preceding 24 hr.

To quantify parasite fitness, as in Figs. 3A & S-3, we divide the per-merozoite reproductive potential into five components:

$$\lambda_t^r = \beta\,\frac{R_t}{M_t}\,Q_t^{ps}, \qquad \lambda_t^e = \beta\,\frac{E_t}{M_t}\,Q_t^{ps},$$
$$\lambda_t^n = \beta\,\frac{R_t+E_t}{M_t}\,Q_t^{pn}, \qquad \lambda_t^w = \beta\,\frac{R_t+E_t}{M_t}\,Q_t^{pw},$$
$$\lambda_t^u = \beta - \lambda_t^r - \lambda_t^e - \lambda_t^n - \lambda_t^w.$$

Here, λ_t^r and λ_t^e are the numbers of offspring that find and successfully reproduce within reticulocytes (immature RBCs) and erythrocytes (mature RBCs), respectively. On the other hand, we have λ_t^n, which is the unrealized potential due to destruction of parasitized cells by the indiscriminate response; λ_t^w, that due to destruction of parasitized cells by the targeted response; and λ_t^u, that due to lack of RBC availability. Note that $\left(\lambda_t^r+\lambda_t^e\right)M_t = M_{t+1}$ and $\lambda_t^r+\lambda_t^e+\lambda_t^n+\lambda_t^w+\lambda_t^u = \beta$.

A. Calculating net change in RBC density. In general, anemia is the result of both (i) the destruction of RBCs and (ii) deficiency in their supply; if the two are balanced, then RBC concentrations remain unchanged. In Figs. 3B & S-3, we compared the previous day's RBC losses, with reticulocyte supply on the following day, computing

$$R_t - (R_{t-1} + E_{t-1})\,(1 - Q^{us}_{t-1})\,.$$

We interpret this quantity as a surplus or deficit according to whether it is positive or negative.

B. Model fitting and smoothing. We began by estimating the ten parameters independently for each mouse using 150 IF2 iterations of 10000 particles. Then, excluding the uninfected mice, we ran 400 iterations of the panel IF2 algorithm (5) using 20000 particles, from each of 250 starting points distributed inside a large box in the 10-dimensional search space. We observed that these algorithms gave estimates clustered in a narrow region of parameter space relative to that spanned by the starting points. To further refine the estimates, we computed a likelihood profile over σ_W, maximizing the likelihood over the remaining parameters at each of 100 values of that parameter. This was accomplished by starting 10 independent IF2 algorithms at each of 100 gridded σ_W values. Each independent IF2 consisted of 3 rounds of 100 iterations of 10000, 20000, and 40000 particles, respectively. The highest observed likelihood overall was taken to be the maximum likelihood estimate (MLE). Smoothed estimates of the state variables were obtained by running 2000 independent particle filter calculations, each using 10^5 particles, and extracting a single trajectory from each one.

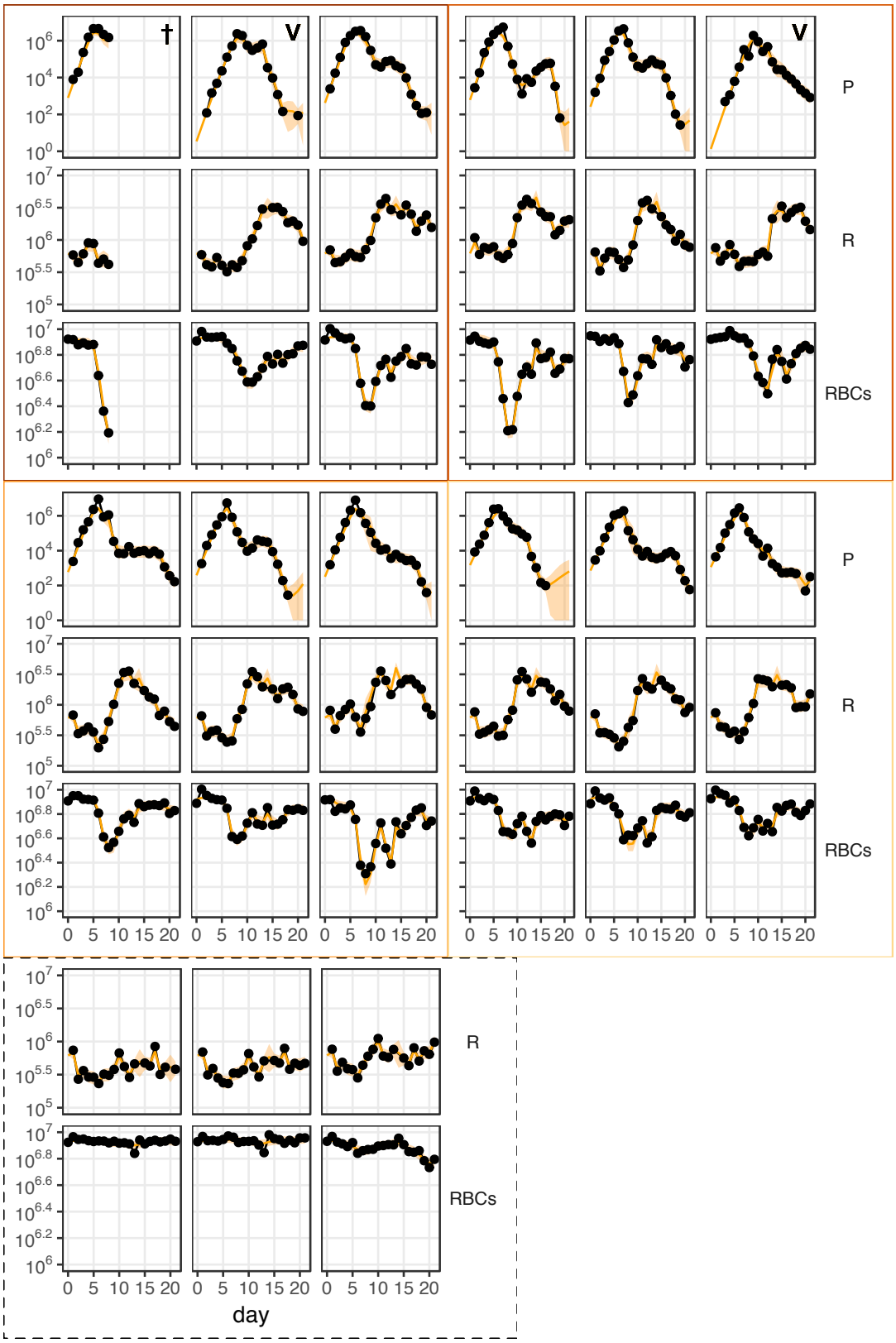

Fig. S-1. Data and fitted model trajectories of each mouse in the study. The density of parasites (P), reticulocytes (R) and total RBCs (RBCs) through time in the fifteen mice used in this study. The model (orange, smooth line) captures the data (black) well, in all cases. Twelve mice (plots with solid border) were infected with one million *Plasmodium chabaudi* parasites. These twelve infected mice were split into four groups of three that received as drinking water a 0.05% (top left block, brown border), 0.005% (top right, light brown border), 0.0005% (middle left, orange border) or 0% (middle right, yellow border) solution of pABA, respectively. Three further mice were left uninfected (bottom left, dashed border). One mouse died (indicated by †) and two received fewer parasites than was intended (V).

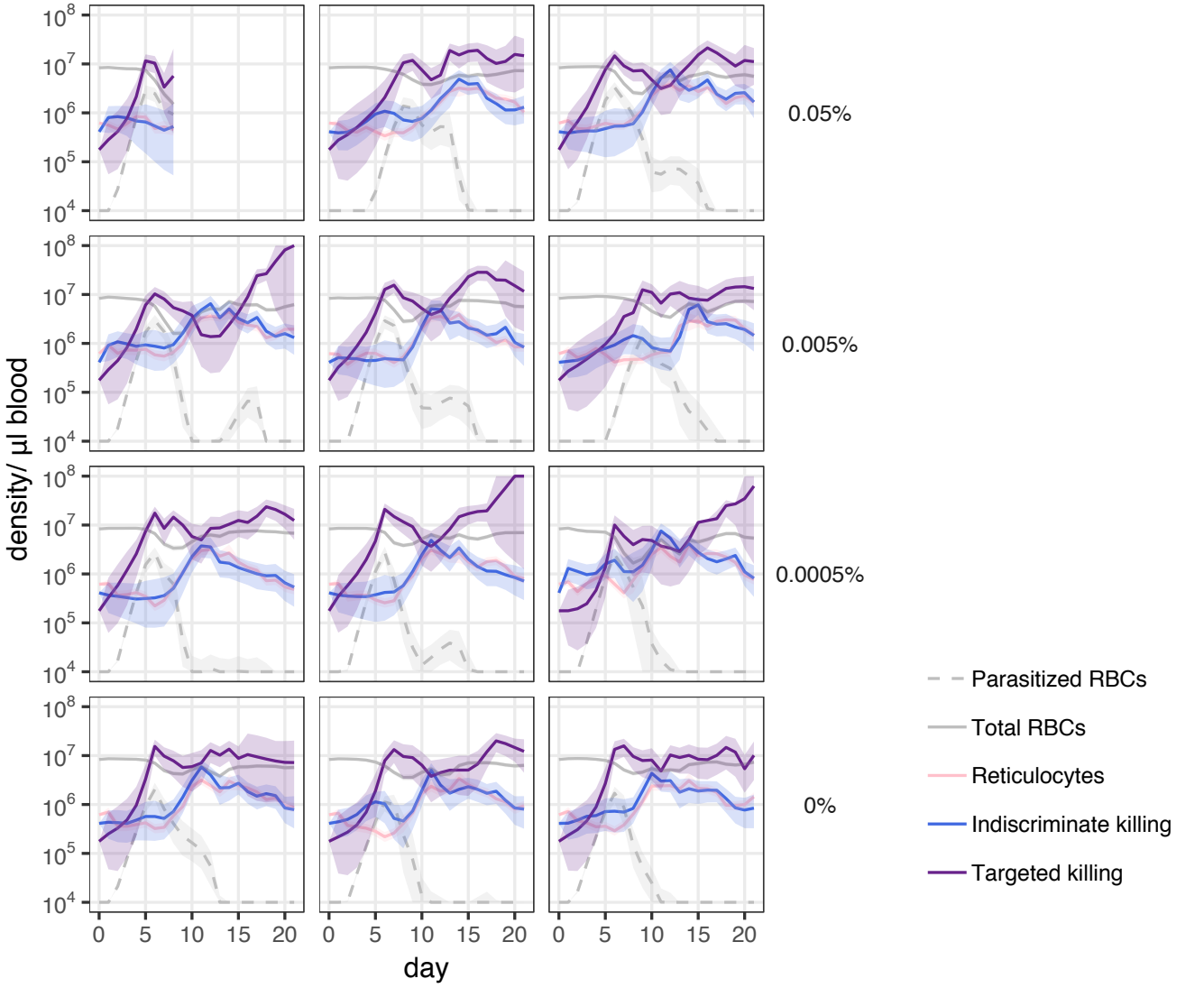

Fig. S-2. Fitted trajectories of the three components of the immune response. The trajectory of the targeted killing response (purple), indiscriminate killing response (blue) and supply response (pink) in each of 12 infected mice; the estimated densities of total RBCs (smooth line) and parasites (dashed line) are shown in grey. Plotted are the mean (solid line) and 90% confidence interval (ribbon) on the smoothed estimate of the model trajectories. Each panel shows the dynamics in a single mouse. The concentration of pABA that each mouse received as drinking water is indicated on the right.

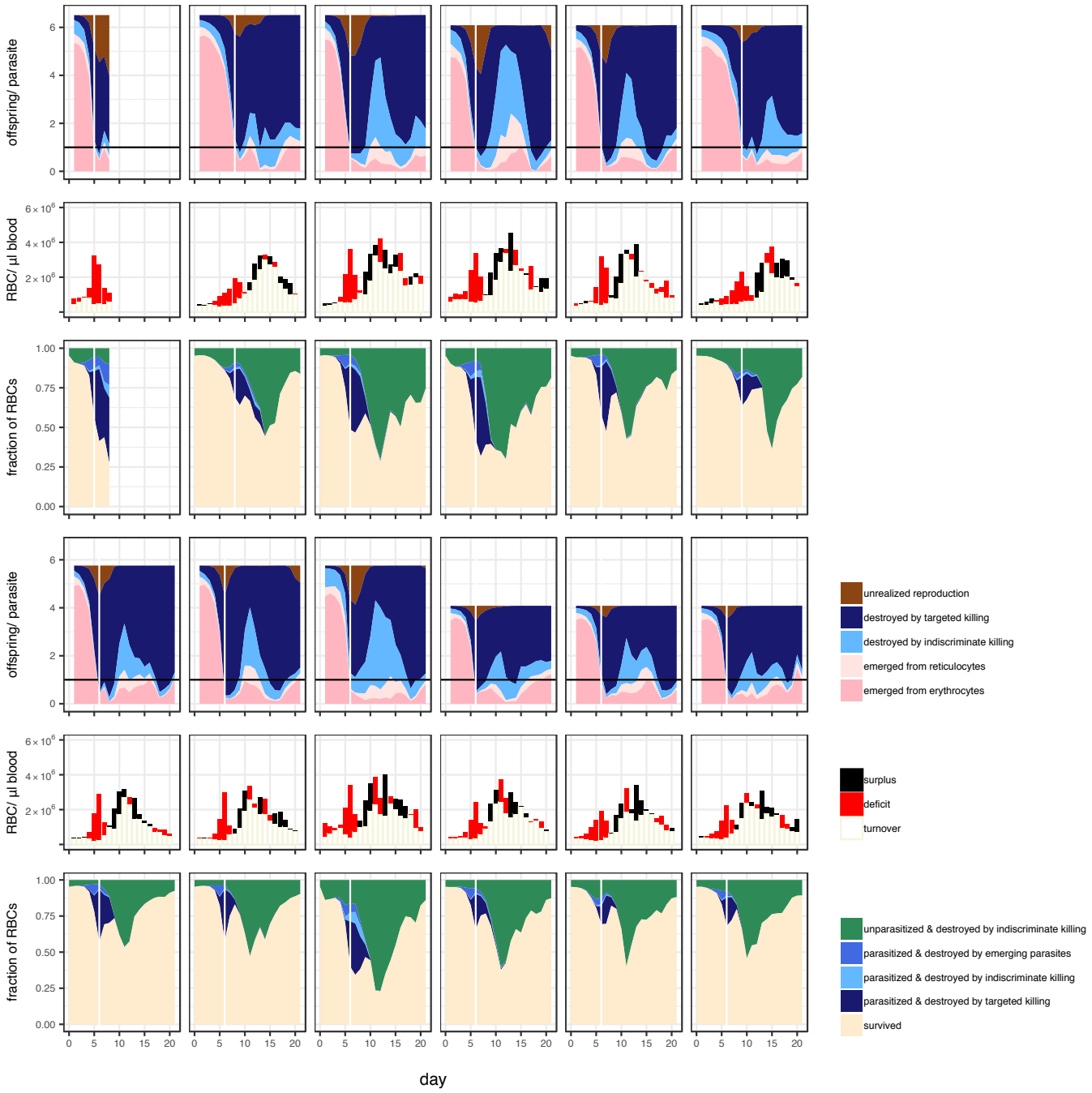

Fig. S-3. Contribution of the different components of the host response to parasite fitness and host disease in each infected mouse. Each column of three plots shows the analysis for a single mouse. First & Fourth row) Contribution of the host to (the suppression of) parasite reproduction. The height of the filled area indicates the maximum number of offspring that could be produced per parasitized cell in conditions of unlimited RBC availability. Fill color indicates the estimated number of offspring that successfully emerged (pinks), were destroyed by each of the killing responses (blues) or were not produced due to the limited availability of RBCs (brown). Black horizontal line indicates one offspring/parasite–when the blue area descends below this line the parasite population is decreasing in size. Second and Fifth Rows) Uncolored part of the bar indicates the number of the previous day's losses that were compensated for by the present day's supply of reticulocytes (turnover); The colored section indicates the extent to which the present day's supply of reticulocytes exceeded yesterday's losses ('surplus', black) or failed to compensate for them ('deficit', red). Third & Sixth Rows) The relative contribution of parasites and each of the host responses to the fate of RBCs through time. Note that parasites can contribute to RBC destruction directly, by emergence, or indirectly via the targeted killing response. White vertical line in A & C indicates the time of peak parasite density. Mice were administered a (top three rows, first three columns) 0.05%, (top three rows, last three columns) 0.005%, (bottom three rows, first three columns) 0.0005% and (bottom three rows, last three columns) 0% solution of pABA as drinking water.

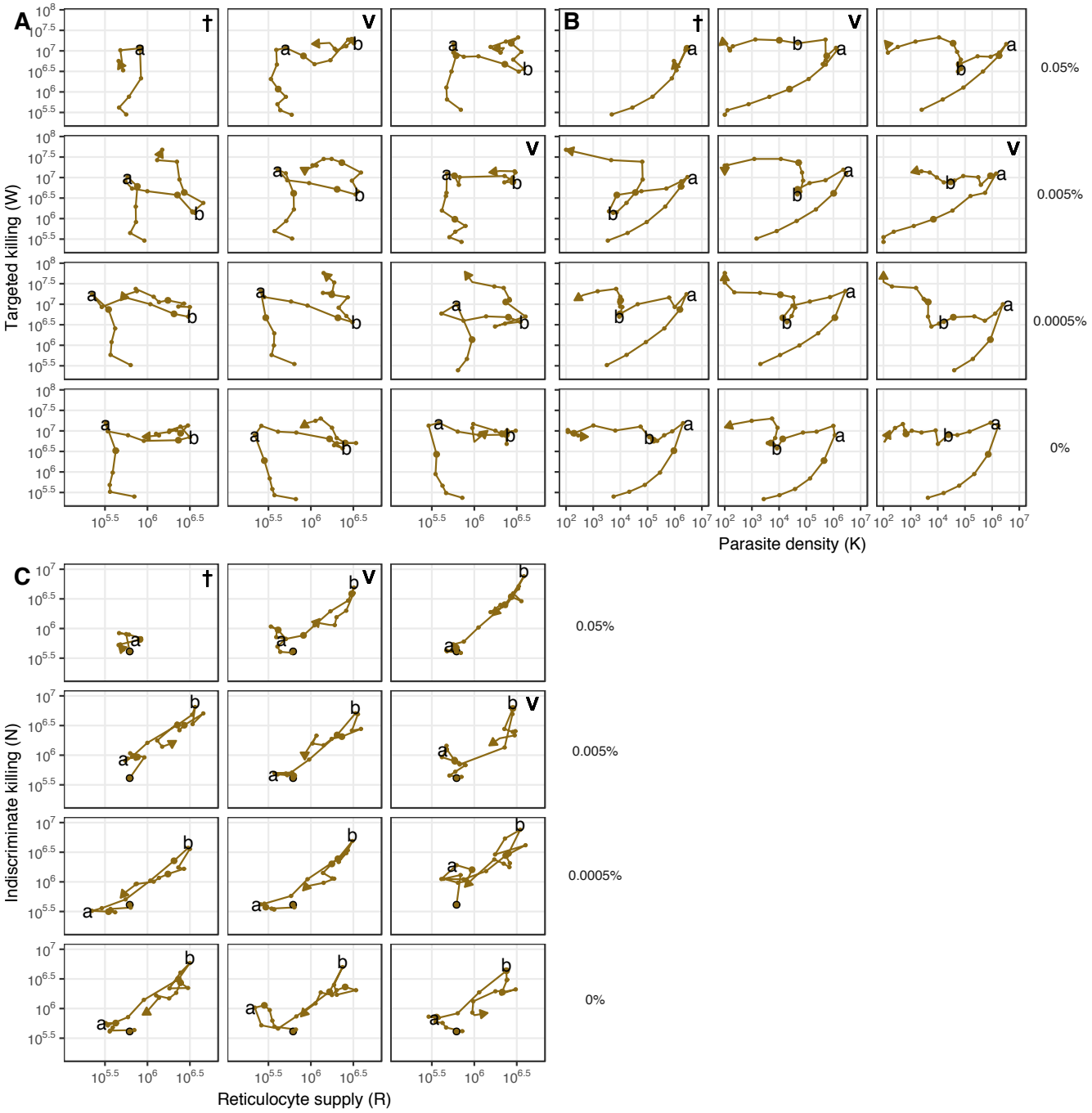

Fig. S-4. The components of the immune response are similarly deployed across mice. The relationships between A) reticulocyte density and targeted killing, B) parasite density and targeted killing and C) reticulocyte density and indiscriminate killing in infected mice given (top row) 0.05%, (second row down) 0.005%, (third row down) 0.0005% and 0% solution of pABA as drinking water. Landmarks **a** and **b** identify transitions between regimens of deployment of the components that occur. In each panel are shown the dynamics of a single mouse. The large, black-lined dot indicates the starting point of the infection; each subsequent day is marked with a dot, with large dots indicating days 5, 10, 15, 20. Densities of parasites and reticulocytes are in units per microliter of blood. Plotted are the median fitted trajectories, as estimated from the model. † indicates that the mouse died (and, as a result, its infection did not extend to landmark **b**), V that the mouse received fewer parasites than was intended.

Table S-1. Flow Cytometer setup

Channel	1	2	3	11
Laser, nm	NA	488	488	785
Emission Filters, nm	NA	430-480	505-560	560-595
Fluorochrome detected	NA	FITC	PE	APC

References

1. BT Pan, R Blostein, RM Johnstone, Loss of the transferrin receptor during the maturation of sheep reticulocytes in vitro. An immunological approach. *Biochem. J.* **210**, 37–47 (1983).
2. J Liu, X Guo, N Mohandas, JA Chasis, X An, Membrane remodeling during reticulocyte maturation. *Blood* **115**, 2021–2027 (2010).
3. T Kina, et al., The monoclonal antibody TER-119 recognizes a molecule associated with glycophorin A and specifically marks the late stages of murine erythroid lineage. *Br. J. Haematol.* **109**, 280–287 (2000).
4. M Koulnis, et al., Identification and analysis of mouse erythroid progenitors using the CD71/TER119 flow-cytometric assay. *J. Vis. Exp.* **54**, e2809 (2011).
5. C Bretó, EL Ionides, AA King, Panel data analysis via mechanistic models. *J. Am. Stat. Assoc.* **in press** (2019).